Global Change Biology

Global Change Biology (2010) **16**, 696–710, doi: 10.1111/j.1365-2486.2009.02028.x

Albedo estimates for land surface models and support for a new paradigm based on foliage nitrogen concentration

D. Y. HOLLINGER*, S. V. OLLINGER†, A. D. RICHARDSON†, T. P. MEYERS‡, D. B. DAIL§, M. E. MARTIN†, N. A. SCOTT¶, T. J. ARKEBAUER‖, D. D. BALDOCCHI**, K. L. CLARK††, P. S. CURTIS‡‡, K. J. DAVIS§§, A. R. DESAI¶¶, D. DRAGONI‖‖, M. L. GOULDEN***, L. GU†††, G. G. KATUL‡‡‡, S. G. PALLARDY§§§, K. T. PAW U¶¶¶, H. P. SCHMID‖‖‖, P. C. STOY****, A. E. SUYKER†††† and S. B. VERMA††††

*Northern Research Station, USDA Forest Service, 271 Mast Rd, Durham, NH 03824, USA, †Complex Systems Research Center, Institute of Earth, Oceans, and Space, University of New Hampshire, Durham, NH, USA, ‡NOAA/ARL/ATDD, Oak Ridge, TN, USA, §Department of Plant, Soil, and Environmental Sciences, The University of Maine, Orono, ME, USA, ¶Department of Geography, Queen's University, Kingston, ON, Canada, ‖Department of Agronomy and Horticulture, University of Nebraska, Lincoln, NE, USA, **Department of Environmental Science, Policy and Management, University of California, Berkeley, CA, USA, ††Northern Research Station, USDA Forest Service, Silas Little, NJ, USA, ‡‡Department of Evolution, Ecology & Organismal Biology, The Ohio State University, Columbus, OH, USA, §§Department of Meteorology, The Pennsylvania State University, University Park, PA, USA, ¶¶Atmospheric & Oceanic Sciences Department, University of Wisconsin - Madison, Madison, WI, USA, ‖‖Department of Geography, Indiana University, Bloomington, IN, USA, ***Department of Earth System Science, University of California – Irvine, Irvine, CA, USA, †††Environmental Sciences Division, Oak Ridge National Laboratory, Oak Ridge, TN, USA, ‡‡‡Nicholas School of the Environment and Earth Sciences, Duke University, Durham, NC, USA, §§§School of Natural Resources, University of Missouri, Columbia, MO, USA, ¶¶¶Department of Land, Air and Water Resources, University of California – Davis, Davis, CA, USA, ‖‖‖Institute for Meteorology and Climate Research, Atmospheric Environmental Research (FZK/IMK-IFU), Garmisch-Partenkirchen, Germany, ****School of GeoSciences, University of Edinburgh, Edinburgh EH9 3JN, UK, ††††School of Natural Resources, University of Nebraska, Lincoln, NE, USA

Abstract

Vegetation albedo is a critical component of the Earth's climate system, yet efforts to evaluate and improve albedo parameterizations in climate models have lagged relative to other aspects of model development. Here, we calculated growing season albedos for deciduous and evergreen forests, crops, and grasslands based on over 40 site-years of data from the AmeriFlux network and compared them with estimates presently used in the land surface formulations of a variety of climate models. Generally, the albedo estimates used in land surface models agreed well with this data compilation. However, a variety of models using fixed seasonal estimates of albedo overestimated the growing season albedo of northerly evergreen trees. In contrast, climate models that rely on a common two-stream albedo submodel provided accurate predictions of boreal needle-leaf evergreen albedo but overestimated grassland albedos. Inverse analysis showed that parameters of the two-stream model were highly correlated. Consistent with recent observations based on remotely sensed albedo, the AmeriFlux dataset demonstrated a tight linear relationship between canopy albedo and foliage nitrogen concentration (for forest vegetation: albedo = 0.01 + 0.071%N, $r^2 = 0.91$; forests, grassland, and maize: albedo = 0.02 + 0.067%N, $r^2 = 0.80$). However, this relationship saturated at the higher nitrogen concentrations displayed by soybean foliage. We developed similar relationships between a foliar parameter used in the two-stream albedo model and foliage nitrogen concentration. These nitrogen-based relationships can serve as the basis for a new approach to land surface albedo modeling that simplifies albedo estimation while providing a link to other important ecosystem processes.

Keywords: albedo, nitrogen, vegetation

Received 16 February 2009 and accepted 31 May 2009

Correspondence: Dr David Y. Hollinger, tel. +1 603 868 7673, fax +1 603 868 7604, e-mail: dhollinger@fs.fed.us

Introduction

The land surface, consisting of vegetation, soil, and snow, is a critical interface of the climate system. It is

Published 2009
This article is a US Government work and is in the public domain in the USA

here that carbon dioxide and other greenhouse gases are absorbed and released, and here that incoming solar radiation is reflected or absorbed and transformed into sensible heat, latent heat, and longwave radiation (Sellers *et al.*, 1997). Land surface models (LSMs) (e.g. Dickinson, 1983; Sellers & Dorman, 1986; Bonan, 1996; Foley *et al.*, 1996; Sellers *et al.*, 1996; Cox *et al.*, 1999; Kucharik *et al.*, 2000; Milly & Shmakin, 2002; Oleson *et al.*, 2004) are integral components of modern atmosphere–ocean general circulation models (hereafter, climate models), and render land surface processes with a high degree of sophistication [see Pitman (2003) for a historical review].

By changing the vegetation present in various grid cells of the underlying LSM, climate models have been used to explore the climatic consequences of historic changes in land use (Bonan, 1997) or changes in surface properties of large-scale features such as the Amazon and boreal forests (Bonan *et al.*, 1992; Henderson-Sellers *et al.*, 1993). More recently, researchers have modified the LSM component of several climate models to address potential climatic consequences of land use strategies (afforestation) aimed at reducing atmospheric CO_2 levels (Betts, 2000; Gibbard *et al.*, 2005; Schaeffer *et al.*, 2006; Bala *et al.*, 2007). In these studies, it was found that in some regions decreases in shortwave radiation reflectivity (albedo) resulting from afforestation contributed to a climatic warming that was greater than the cooling effects of reduced atmospheric carbon dioxide associated with growth of these forests.

These results highlight the importance of the albedo component of LSMs, an area of relative neglect for the last 20 years. Although great strides have been made during this time in modeling canopy photosynthesis and evapotranspiration, soil and snow thermodynamics, and hydrology (e.g. Sellers *et al.*, 1996; Dai & Zeng, 1997; Oki & Sud, 1998; Kucharik *et al.*, 2000; Bonan *et al.*, 2002; Dai *et al.*, 2003; Friend & Kiang, 2005; Thornton & Zimmermann, 2007), the albedo component of most LSMs has changed little. At the same time, albedo data have increased enormously from observational networks (e.g. Baldocchi *et al.*, 2001) and newer techniques are available to constrain model parameters from data (Tarantola, 2005).

The surface albedo, α, is a fundamental component of the net surface energy balance, R_n,

$$R_n = s(1-\alpha) + \vartheta_a - \vartheta_s, \tag{1}$$

where s is the shortwave solar energy, ϑ_a is the longwave radiation emitted by the atmosphere, and ϑ_s is the longwave radiation emitted by the surface. LSMs generally use one of two schemes for generating vegetated surface albedos; (1) simple schemes prescribing albedo based on the classification of the surface vegetation (e.g. Manabe, 1969; Dickinson *et al.*, 1986; Milly & Shmakin, 2002), or (2) a calculation of albedo using an approximation of canopy radiation transport. In these approximation methods, instead of solving the full transport equation, the canopy is assumed horizontal, and the radiation field is divided into several components (Myneni *et al.*, 1989). The simplest approach is to separate the radiation into upward and downward propagating diffuse streams based on the equations of Kubelka and Munk (see Kubelka, 1948). Dickinson (1983) and Sellers (1985) developed a model that combined the direct solar beam with diffuse radiation into two streams. In other treatments of escalating complexity, additional streams of radiation are considered; the direct solar component as a third stream (Allen *et al.*, 1970b), and in the remote sensing field, the radiation in the view direction as a fourth stream (Suits, 1972; Verhoef, 1984).

The two-stream model of Sellers (1985) was incorporated into the Simple Biosphere Model (Sellers & Dorman, 1986) and has been widely applied in other LSMs. In this model and its offspring, the surface albedo depends on solar elevation, the proportion of solar radiation that is diffuse, vegetation-specific optical properties, the canopy leaf and stem leaf area indices, and the soil or understory albedo (Dorman & Sellers, 1989; Bonan, 1996). Because foliage reflectance and transmittance is generally low ($<10\%$) over visible wavelengths (400–700 nm) but high ($>30\%$) in the near infrared (NIR) (700–2500 nm), these wavebands are treated separately in the two-stream approach.

Albedo data used to characterize different vegetation or plant functional types (PFTs) for both the prescriptive and two-stream approaches have generally come from summaries (e.g. Mathews, 1984; Henderson-Sellers *et al.*, 1986) of earlier primary sources such as Federer (1968). These early studies often included data for only a limited portion of the annual cycle (sometimes only a few days) and provide limited or no replication within a PFT. Albedos of some vegetation types were not available and were thus estimated from other vegetation types that were assumed to be 'similar.' Leaf level parameters for the two-stream used in LSMs still rely on coarse estimates that have not changed since Dorman & Sellers (1989), even though these authors long ago suggested that improved parameterizations could be obtained by inverting the model against additional field albedo data.

Here, we use over 40 site-years of data from the AmeriFlux network (Law *et al.*, 2002) to examine forest, crop, and grassland albedo parameterizations of several LSMs and use inverse methods to suggest several improved parameterizations. This is a far more comprehensive dataset than used in previous estimates of albedo, providing continuous replication within functional types and across years. Here, we limit the

discussion to growing season (snow-free) albedo, although the data sources and inverse methods apply equally well to evaluating commonly used snow albedo model formulations. Finally, recent results based on remotely sensed albedo demonstrated that much of the variation in growing season albedos for temperate and boreal forests could be related to variation in canopy nitrogen concentration (Ollinger *et al.*, 2008). Following this result, we compared foliage nitrogen concentrations with field-measured albedo and examined the potential utility of this relationship for improvement of albedo parameterizations.

Materials and methods

Study sites and available data

Sites used in the analysis were part of the AmeriFlux network and included a range of deciduous and evergreen forests, grazed and ungrazed grasslands, and tilled croplands (Table 1). For each site, albedo and other data were obtained from sensors mounted on towers extending 2–10 + m above intact vegetation. Downward and upward global shortwave radiation were measured with Kipp and Zonen CNR1 four-component radiometers (Kipp & Zonen, Delft, the Netherlands) which feature ISO second class pyranometers. On a subset of sites, upward and downward photosynthetically active radiation (PAR) data were measured with LiCor LI-190 (Li-Cor, Lincoln, NE, USA) or Kipp and Zonen PAR-lite sensors. The percent diffuse radiation was recorded with a Delta-T model BF-3 Sunshine sensor at three sites. Measurements of up- and down-welling radiation were recorded at 1–30 s intervals and averaged over 30 or 60 min.

Albedo calculations and parameter estimation

For comparisons between vegetation types, mean albedos were calculated as

$$\alpha = \frac{\sum s_{\text{out}}}{\sum s_{\text{in}}}, \tag{2}$$

where the summation of incoming (s_{in}) or outgoing radiation (s_{out}) was carried out over a specified time period.

Leaf and canopy parameters were estimated for the two-stream canopy radiative transfer model described in Dickinson (1983) and Sellers (1985), as modified by

Table 1 Data sources used in this study

Site and year	Vegetation	Leaf area index	Latitude, longitude	PFT	Site reference
Bartlett forest (2005)	Beach/maple/birch	4.5	44.0646°N, 71.2881°W	BDT	Jenkins *et al.* (2007)
Chestnut Ridge (2006)	Oak/hickory	4.5	35.9311°N, 84.3324°W	BDT	
Duke hardwoods (2004)	Oak/hickory	5.6	35.9736°N, 79.1004°W	BDT	Stoy *et al.* (2005)
Morgan Monroe (2004)	Maple/tulip poplar/oak	4.9	39.3232°N, 86.4131°W	BDT	Schmid *et al.* (2000)
Silas Little (2004)	Oak	4.7	39.9137°N, 74.5960°W	BDT	Skowronski *et al.* (2007)
UMBS (2006)	Poplar/maple/birch	4.4 ('05)	45.5598°N, 84.7138°W	BDT	Gough *et al.*, (2008)
Willow Creek (2005)	Maple/basswood/ash	5.4	45.8059°N, 90.0799°W	BDT	Cook *et al.* (2004)
Ozark (2005)	Maple/oak/hickory	4.0	38.7441°N, 92.2000°W	BDT	Gu *et al.* (2006)
Howland (2008)	Japanese larch	2.5	45.2163°N, 68.7097°W	NDT	
Black Hills (2005)	Ponderosa pine	2	44.158°N, 103.650°W	NET	
Duke pine (2004)	Loblolly pine	2.5–5.2	35.9782°N, 79.0942°W	NET	Stoy *et al.* (2005)
Ft. Dix (2006)	Pitch pine/oak		39.9712°N, 74.4345°W	NET	Skowronski *et al.* (2007)
Howland (2007)	Spruce/hemlock	4.7–5.7	45.2041°N, 68.7403°W	NET	Hollinger *et al.* (2004)
Wind River (2006)	Douglas fir/hemlock	8	45.8205°N, 121.9519°W	NET	Paw *et al.* (2004)
1930 Burn	Black spruce	7.2	55.8205°N, 121.9519°W	NET	Goulden *et al.* (2006)
1851 Burn NOBS	Black spruce	5.5	55.8205°N, 121.9519°W	NET	Goulden *et al.* (2006)
Brookings	Ungrazed pasture	0.2–3	44.3453°N, 96.8362°W	C3G	
Canaan	Pasture	1–3	39.0633°N, 79.4208°W	C3G	
Goodwin Creek	Pasture	2	34.25°N, 89.97°W	C3G	
Vaira	Pasture	1–2.7	38.41°N, 120.95°W	C3G	Baldocchi *et al.* (2004)
Mead irrigated continuous	Maize (no till)	5.5	41.1651°N, 96.4766°W	Crop	Verma *et al.* (2005)
Mead irrigated rotation	Maize (no till)	6	41.1649°N, 96.4701°W	Crop	Verma *et al.* (2005)
Mead irrigated rotation	Soybean (no till)	5.5	41.1649°N, 96.4701°W	Crop	Verma *et al.* (2005)
Mead rainfed rotation	Maize (no till)		41.1797°N, 96.4396°W	Crop	Verma *et al.* (2005)
Mead rainfed rotation	Soybean (no till)		41.1797°N, 96.4396°W	Crop	Verma *et al.* (2005)
Bondville rotation	Maize (no till)	5.5	40.0061°N, 88.2919°W	Crop	
Bondville rotation	Soybean (no till)	5	40.0061°N, 88.2919°W	Crop	

NDT, needle-leaf deciduous tree; BDT, broadleaf deciduous trees; NET, needle-leaf evergreen trees ; PFT, plant functional type.

Bonan (1996), and using the notation and form of Oleson *et al*. (2004). This is a one-dimensional approach lacking crown geometry or any consideration of leaf clumping. In this model, upward and downward diffuse fluxes of radiation are tracked separately as functions of the incident diffuse plus direct flux in two coupled linear differential equations based on the approach of Coakley & Chýlek (1975)

$$-\bar{\mu}\frac{\partial I\uparrow(L)}{\partial L}+[1-(1-\beta)\omega]I\uparrow-\omega\beta I\downarrow = \omega\bar{\mu}K\beta_0 e^{-K(L+S)}, \quad (3)$$

$$\bar{\mu}\frac{\partial I\downarrow(L)}{\partial L}+[1-(1-\beta)\omega]I\downarrow-\omega\beta I\uparrow = \omega\bar{\mu}K(1-\beta_0)e^{-K(L+S)}. \quad (4)$$

Optical depth is represented by leaf area index (L) [or leaf plus stem area (S) index], $I\uparrow$ and $I\downarrow$ are the upward and downward diffuse radiation fluxes per unit incident flux, $\bar{\mu}$ is the average inverse diffuse optical depth per unit leaf area (this depends upon χ, the departure of leaf angles in the canopy from a random orientation), ω is a scattering coefficient, β and β_0 are upscatter parameters for diffuse and direct beam radiation, and

$$K = G(\mu)/\mu, \quad (5)$$

where μ is the cosine of the zenith angle of the incident beam of solar radiation and $G(\mu)$ is the relative projected leaf area in the direction $\cos^{-1}(\mu)$ (Ross, 1981). Given boundary conditions of the incident radiation at the top of the canopy and ground surface direct and diffuse radiation albedos, these equations were solved by Sellers (1985) to generate expressions for surface albedos, the amount of radiation reaching below the canopy, and estimates of the amount of radiation absorbed by the canopy for further calculations of photosynthesis and transpiration. Because foliage absorbs radiation much more strongly in the photosynthetically active region (400–700 nm) than NIR (700–2500 nm), these equations are evaluated separately for these two bands with two sets of parameters for β, β_0, and ω.

The scattering coefficient ω_Λ for waveband Λ (where Λ = vis for the 400–700 nm band or NIR for the 700–2500 nm band) is a weighted combination of leaf and stem reflectances (α) and transmittances (τ),

$$\omega_\Lambda = L/(L+S)\alpha_\Lambda^{\text{leaf}} + S/(L+S)\alpha_\Lambda^{\text{stem}} + L/(L+S)\tau_\Lambda^{\text{leaf}} + S/(L+S)\tau_\Lambda^{\text{stem}}. \quad (6)$$

The canopy upscattering parameters β and β_0 are defined in terms of the scattering coefficient [Eqn (6)] and relations that take into account solar elevation (for the direct beam upscatter coefficient) and the leaf angle distribution. The diffuse upscatter coefficient also directly incorporates combined leaf and stem reflectance and leaf and stem transmittances. The model is thus formulated in 11 parameters, eight at the 'leaf-level' (α_{vis}, α_{NIR}, τ_{vis}, and τ_{NIR} each for leaves and stems) and three canopy-level or 'structural' parameters, (L, S, and χ). Note that the degree to which foliage is clumped is sometimes considered an additional parameter; in this version of the model the foliage is not clumped but randomly located (Myneni *et al*., 1989).

Of the eight leaf-level parameters, four of them are incorporated in the visible scattering coefficient (ω_{vis}) and another four are incorporated in the NIR scattering coefficient (ω_{NIR}). This structure allows different combinations of parameters to generate identical values for the scattering coefficient (and ultimately albedo) and creates difficulties for model inversion. This also means that there are effectively fewer leaf-level parameters than specified – we discuss this in more detail later. Dorman & Sellers (1989) provided estimates of the eight leaf-level parameters and for a variety of vegetation types; these values remain unchanged in the present technical description of the Community Land Model in Oleson *et al*. (2004 Table 3.1). The seasonal progression of leaf area index and stem area index are prescribed for different plant function types (Bonan, 1996). The model requires a lower boundary (soil) albedo, in these simulations this was fixed at 0.15.

At three sites [representing needle-leaf evergreen trees (NETs), broadleaf deciduous trees (BDTs), and deciduous needle-leaf trees] we had sufficient data to carry out inversion-based estimates of model parameters. Required data consisted of half-hourly upward and downward shortwave radiation, upward and downward PAR, diffuse fraction, and solar elevation. Forest floor albedo was fixed at 0.15 in these simulations. Two-stream model parameters were estimated by the Monte Carlo method using the Metropolis algorithm. Model and data were compared for half-hourly data recorded in July and encompass a range of solar elevations and diffuse/direct ratios but constant leaf and stem areas. Optimizing this model presents several challenges; the model calculates albedo in the photosynthetically active (vis) and NIR bands yet measurements are only available for visible and total shortwave (350–2500 nm) radiation. Based on integration of clear sky temperate latitude summer spectral irradiances (Gueymard, 2004), we assumed that incoming solar radiation was split 46/54 between the vis (including UV) and NIR bands. Because the climate system is sensitive to the disposition of energy (which varies across bands), and not reflectance *per se*, we weighed

the half-hourly albedo mismatch between data and model in the summation of the cost function [Eqns (7) and (8)] by the incoming shortwave radiation s. This means that clear sky mid-day measurements are properly weighed compared with overcast or early and late day measurements. Cost functions (G_{vis} and G_{sw}) were evaluated using both PAR albedo (to obtain parameters in the visible band) and PAR albedo plus shortwave albedo to obtain NIR parameters,

$$G_{vis} = \sum s(F_{vis} - a_{vis})^2, \quad (7)$$

$$G_{sw} = \sum s(0.46F_{vis} + 0.54F_{NIR} - a_{sw})^2, \quad (8)$$

where F_{vis} and F_{NIR} represent two-stream model albedos for visible and NIR radiation at the same half-hour as the a_{vis} and a_{sw} measurements. Inputs to the model are L, S, μ (cosine of the solar zenith angle), and the proportion of the radiation that is diffuse. The later is used to weigh the reflected direct and diffuse fluxes for contribution to the total reflected flux. Because our objectives were to obtain good model performance for both visible and total shortwave albedos, we calculated a Pareto optimum in which parameters leading to a decrease (improvement) in one cost function were only accepted if they did not cause an increase (worsening) in the other cost function.

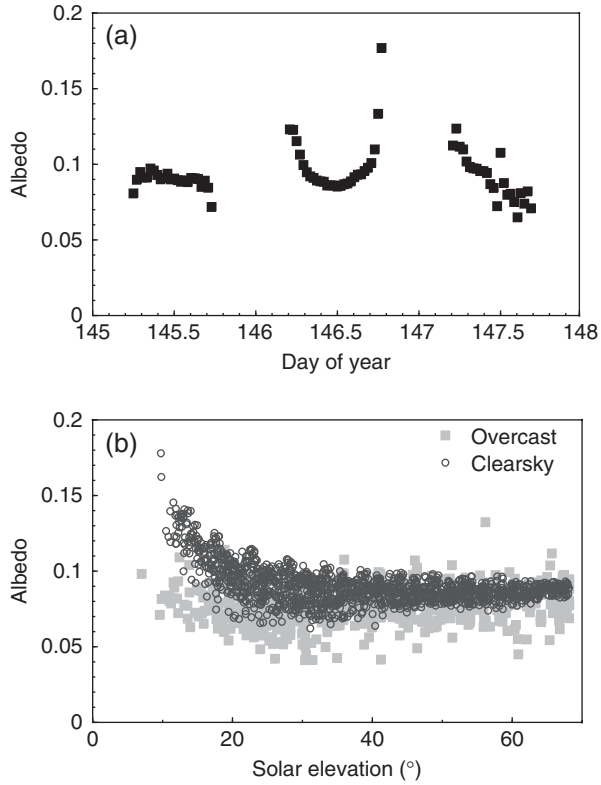

Fig. 1 (a) Variation in shortwave albedo of spruce-hemlock forest over several days. (b) Albedo as a function of solar elevation for clear sky (open circles, <40% diffuse) and overcast conditions (gray squares, >95% diffuse).

Results and discussion

General patterns of observed albedo

Observed growing season surface albedos ranged from <0.05 to over 0.25 across sites and also showed considerable within-site variation as a function of sun angle and illumination conditions. Data from an evergreen forest illustrates that when skies are clear (e.g. day 146 in Fig. 1a), half-hourly integrated albedos decreased with increasing sun elevation (Fig. 1b). In contrast, on overcast days (e.g. day 145, Fig. 1a) when incoming radiation is isotropic, albedos were constant (Fig. 1b). Shortwave albedo was generally lower under overcast conditions than under clear skies. When albedo was integrated over a day, variations in the amount and timing of cloudiness still caused considerable day-to-day variation (blue and red dots, Fig. 2), although these variations were smoothed out when albedo was integrated over several weeks (Fig. 2, lines).

A comparison of albedo values across forested sites shows wide variations in absolute albedo and seasonal patterns between sites (Fig. 2). When foliage is present, deciduous forest albedo can be more than twice that of evergreen conifers. Deciduous forest albedos are also more seasonally variable than evergreen forest albedos. In the AmeriFlux data, deciduous forest albedos increase by 20–50% from spring lows to seasonal maxima, a transition that occurred within about 30–40 days as

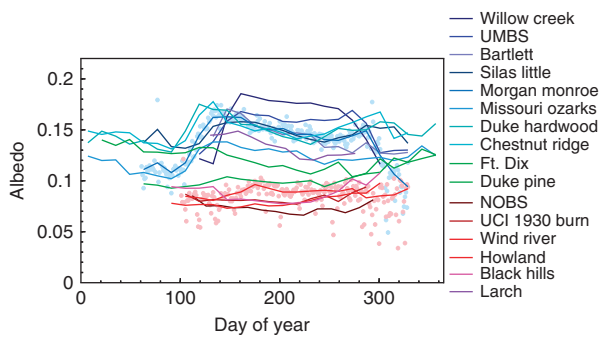

Fig. 2 Snow-free seasonal albedos integrated over a 2-week period (solid lines) and integrated over 1 day (dots). Blue lines signify temperate, broadleaf deciduous trees, green lines, pine forest (needle-leaf evergreen trees), red lines, evergreen conifer forest (needle-leaf evergreen trees), and purple line, larch forest (deciduous needle-leaf trees). The lengths of the various lines are coincident with the snow-free season at each site. The blue dots indicate daily albedo at the Morgan Monroe site, the red dots at the Howland forest.

the foliage expanded (Fig. 2). The beginning of canopy development occurred around day 100 at the southern-most sites (Duke and Chestnut Ridge), preceding that of the northern-most sites (Willow Creek, UMBS, and Bartlett) by 30–40 days ($\sim$ 4 days per degree latitude). Following a spring maximum of $\sim$ 0.14 (Ozark) to $\sim$ 0.18 (Willow Creek), deciduous forest albedos declined gradually through the summer before declining more rapidly around day 280 (northern sites) and 20–30 days later at the southern sites. At many of the deciduous sites, albedo increased slightly in the early fall before decreasing; presumably leaf reflectance and transmittance in the visible wavelengths increased as a result of the destruction of chlorophyll. Mid-summer albedos for broadleaf deciduous forests varied by more than 30% across sites, from $\sim$ 0.13 at the Ozark site to $\sim$ 0.17 at Willow Creek. The two sites with the highest growing season albedos were also the most northerly.

When integrated over 3 months and averaged between sites, the albedo of the broadleaf deciduous forest type (Table 2) is similar for the spring, summer, and fall seasons at about 0.15. This constancy is an artifact of averaging southerly sites and more northerly sites. In the spring, leaf-out and an albedo increase takes place at the southerly sites in April, compensating for the lower albedos of the northerly sites. A similar phenomenon occurs in the autumn (Fig. 2).

Evergreen needle-leaf forest albedos were lower than broad-leaf deciduous forest albedos, with the exception of the Duke loblolly pine site where winter values were greater than several of the leafless hardwood sites (Fig. 2). The pines at the southern-most sites (Duke and Ft. Dix) had consistently higher albedos than the more northerly conifer forests. When averaged across a season, albedos at these more southerly sites were about 0.11, 60–70% that of deciduous forest, whereas consistent with other reports (e.g. Betts & Ball, 1997), the

Table 2 Land Surface Model Albedos

PFT	This study	Mathews*	HS†	Milly‡	Dickinson§	Cox¶
Spring (April–May)						
BDT	0.145 (0.012)	0.12	0.19	0.13	0.18	0.13
NDT	0.145	–	–	0.13	0.14	0.13
BET	–	0.11	0.11	0.13	0.12	0.12
NET	0.084 (0.006) northerly 0.111 (0.018) southerly	0.12	0.13	0.11	0.14	0.14
Grassland	0.209 (0.021)	0.20	0.19	0.20	0.20	0.19–0.20
Crop	0.178 (0.013)		0.20	0.16	0.2	0.17–0.25
Summer (June–August)						
BDT	0.152 (0.013)	0.15	0.19	0.13	0.18	0.13
NDT	0.133	–	–	0.14	0.13	0.13
BET	–	0.11	0.11	0.13	0.12	0.12
NET	0.079 (0.007) northerly 0.105 (0.018) southerly	0.15	0.13	0.11	0.14	0.14
Grassland	0.181 (0.008)	0.20	0.19	0.20	0.20	0.19–0.20
Crop	0.189 (0.020)		0.20	0.16	0.2	0.17–0.25
Fall (September–October)						
BDT	0.146 (0.015)	0.12	0.19	0.13	0.18	0.13
NDT	0.127	–	–	0.13	0.13	0.13
BET	–	0.11	0.11	0.13	0.12	0.12
NET	0.089 (0.006) northerly 0.107 (0.004) southerly	0.11	0.13	0.11	0.14	0.14
Grassland	0.197 (0.008)	0.18	0.19	0.20	0.20	0.19–0.20
Crop	0.193 (0.018)		0.20	0.16	0.2	0.17–0.25

Values in parentheses represent one standard deviation of the mean.
*Mathews (1984), used in GISS models.
†Henderson-Sellers *et al*. (1986).
‡Milly & Shmakin (2002), used in GFDL-CM2.
§Dickinson *et al*. (1986), used in BATS.
¶Cox *et al*. (1999), used in UKMO-HadCM3.
NDT, needle-leaf deciduous tree; BDT, broadleaf deciduous trees; NET, needle-leaf evergreen trees; PFT, plant functional type; BET, broad-leaf evergreen tree.

albedo at the more northerly conifer sites averaged between about 0.08–0.09, only ~50–60% that of the mean deciduous forest values (Table 2). There is no clear signal of canopy phenology as evidenced by spring increase or autumn decline in any of the evergreen conifer albedos. The general pattern seen at the different sites of a mid-year minimum is presumably due to the impact of higher solar elevations in the summer.

The deciduous needle-leaf tree (larch) seasonal albedo exceeded all other conifers (Fig. 2) and overlaps the albedo range seen in BDTs. Seasonal variation of larch albedo resembles that of a broadleaf deciduous forest more than an evergreen needle-leaf forest (Fig. 2).

Consistent with our earlier findings (Ollinger *et al.*, 2008), the wide range of midsummer forest albedos among sites does not appear to be caused by differences in leaf area index, which were generally well above 2 (Table 1). Albedo generally changes little above a leaf area index of ~3 (Asner, 1998, and see Fig. 8b).

The growing season albedos of grassland and crop surfaces generally exceed those of forests (Fig. 3 and Table 2), although there was overlap between grassland albedo and those of the highest albedo forests (compare Figs 2 and 3a). The Mediterranean climate (summer drought) Vaira grassland site was qualitatively different from the other (temperate) grassland sites. The temperate grassland site albedos reached a minimum near the middle of summer. By contrast, the crop sites tended to show late summer maxima in albedo. Although maize and soybean albedos were similar at the beginning of

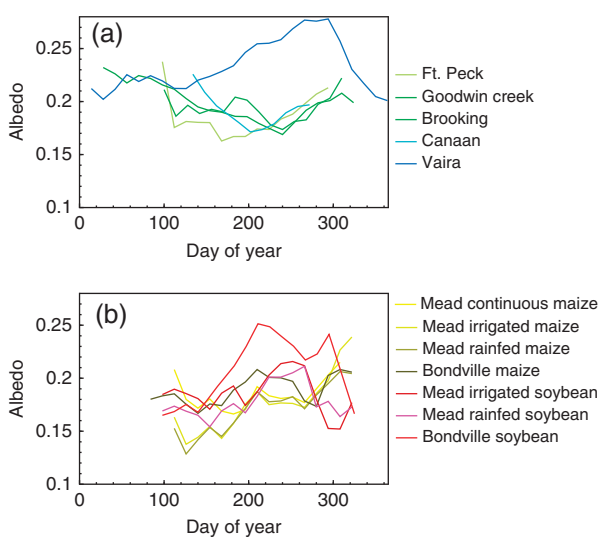

Fig. 3 Snow-free seasonal albedo integrated over 2-week periods for grasslands (a) and crops (b). Where multiple years of albedo data are available (e.g. Ft. Peck, Goodwin Creek), data from the year with the median albedo value for the biweekly period nearest day 200 are shown.

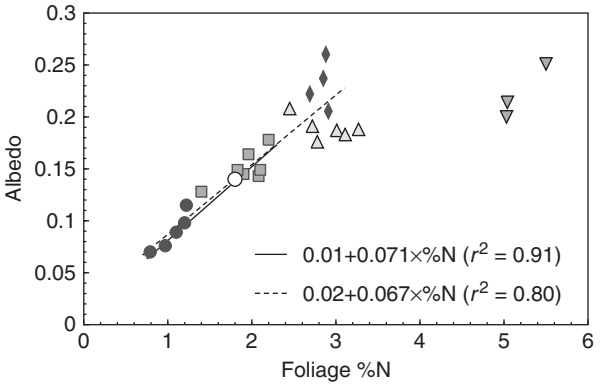

Fig. 4 Relationship between foliage nitrogen concentration and canopy shortwave albedo calculated for the biweekly period nearest day 200. Symbols: black circles, needle-leaf evergreen trees (NET); squares, deciduous broadleaf trees (BDT); white circle, needle-leaf deciduous trees (NDT); triangles, maize; upside down triangles, soybeans; diamonds, grass. The solid line is a regression of trees only, the dashed line includes all data except soybean.

the growing season, presumably because most reflectance at this time was from the soil surface, soybean canopies had significantly higher albedos than maize grown on the same site throughout much of the summer. However, during the fall when post harvest debris lay in the fields, this pattern reversed and maize residue albedos were greater than soybean. Specifically, soybean albedos were ~20% higher than maize at both Bondville, Illinois, and Mead, Nebraska, in August but about 20% lower in October. When averaged between sites and over a season (Table 2), grassland albedos were slightly lower in the summer at about 0.18 than in spring or fall (~0.20).

Field measurements of site foliage nitrogen concentration were good predictors of integrated (2-week period) mid-summer albedo (Fig. 4), $r^2 > 0.8$, $P < 0.001$. This relationship seems to be similar for different tree functional types (RMA regressions for needle-leaf trees, $\alpha = 0.100\%\text{N}-0.02$, $P = 0.002$, for BDTs, $\alpha = 0.061\%\text{N} + 0.03$ $P = 0.058$, for all trees, $\alpha = 0.071\%\text{N} + 0.01$, $P < 0.001$; note that none of the intercepts are significantly different from zero) and generally held for other functional types at higher nitrogen concentrations. For nitrogen concentrations of less than about 3%, this relationship was linear with albedo increasing by approximately 0.067 with each percent increase in nitrogen (Fig. 4, all sites except soybeans, dashed line; forests only, solid line). The relationship between nitrogen and albedo appeared to saturate at higher foliage nitrogen concentrations (Fig. 4). Many of the differences seen between forested sites in Fig. 2 appear to be explicable based on foliage nitrogen differences, suggesting

that the simple regressions in Fig. 4 might find wide application.

Comparison of tower albedos to values used in climate models

A variety of climate models have been used to forecast the future state of the climate system (see Randall *et al*., 2007 for summary) and these models employ several different albedo formulations. Many (e.g. GFDL-CM2, UKMO-HadCM3, GISS) specify albedos that depend on a broad grouping of vegetation functional types such as BDTs, grassland, or crops. In some cases (e.g. models based on data from Mathews, 1984), a slight seasonal variation in albedo is incorporated. For the BDT vegetation type, the albedo values used by Mathews (1984), Milly & Shmakin (2002), and Cox *et al*. (1999) are within 2 SD deviations of our seasonal means, although $\sim$ 10–15% below our mean. Values suggested by Henderson-Sellers *et al*. (1986) and Dickinson *et al*. (1986) for BDT albedo are more than 2 SD ($\sim$ 20–30%) above the mean value from our observations. For the NET type, all models use albedos that are well above our values for northerly evergreen forests (boreal and sub-boreal) but representative of more temperate pine forests. The large difference in albedo between these two types of needle-leaf evergreen trees ($\sim$ 25%) and their geographically distinct locations suggest that it may be useful for climate modelers to subdivide the evergreen needle-leaf tree type. The mean seasonal grassland and crop surface albedos used in a number of climate models are consistent with the results reported here (Table 2).

As described earlier, climate models that calculate albedo based on the Sellers (1985) two-stream approach use a series of nine parameters for each functional type as well as monthly values of leaf and stem area index. Because direct and diffuse radiation scatter differently in a canopy, these calculations also require the solar elevation and a separation of direct and diffuse radiation. We used the proportioning of diffuse and direct radiation recorded at the Bartlett site because this separation was not available at most locations (results based on the proportions of direct and diffuse radiation recorded at the Howland site gave nearly identical results).

The two-stream model generally provided vegetation functional type albedo estimates that are consistent with this synthesis (Fig. 5). The two-stream model estimates during the growing season are generally within the 95% confidence intervals of the ensemble means of the temperate broad leaf tree (BDT-TEM), NET, and crop functional types. During the autumn, however, the two-stream model predicts a significant reduction in albedo for the BDT-TEM functional type that is often not observed. An examination of the two-stream model driving variables (Bonan, 1996) shows that in the September–October period the leaf area index drops while the stem area index increases (the change in stem area index presumably is to simulate the changing color of senescing deciduous tree canopies). However, the optical properties of stems used by this life-form (Dorman & Sellers, 1989) are such that they are considerably darker than foliage, accounting for the excessive decline in Fig. 5a.

A more dramatic under-prediction by the model occurred for the needle-leaf deciduous tree (NDT) functional type (Fig. 5c). Data from this functional type were

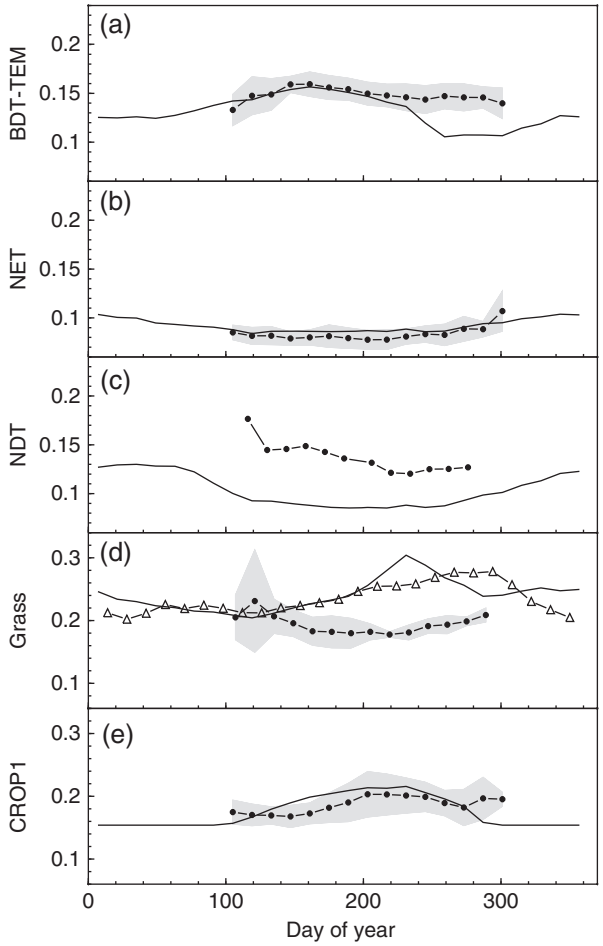

Fig. 5 Growing season shortwave albedos for various plant functional types calculated from AmeriFlux sites. Gray region represents 95% confidence interval for biweekly means (dots). The solid line represents seasonal (snow-free) albedos calculated via the two-stream albedo model of Sellers (1985) as implemented in the Community Land Model (Oleson *et al*., 2004). For the grass functional type (D) the black dots represent the mean value for four temperate grasslands while the open triangles indicate albedo measurements of Mediterranean grassland.

not available to Dorman & Sellers (1989) when they published their foliage optical parameters and were thus set equal to those of NETs. Although additional data are needed to confirm our results, we suggest that the two-stream NDT functional type albedo estimates are only about two-thirds of correct values. Interestingly, NDT estimates for models using fixed parameterizations (Table 2) are much closer to our results. In the case of grass canopies, the two-stream model more closely simulates the Mediterranean Vaira site than the other temperate grasslands (Fig. 5d). For the temperate sites the two-stream model dramatically overpredicts grassland albedo in the summer and early fall; by August, the two-stream model predicts an albedo of ~ 0.3, about 50% higher than measured values. This over-prediction can be traced to the increasing proportion of senescent material (stem area index) that contributes to the overall canopy structure later in the summer. Unlike in the case of woody vegetation, the optical properties of grass stems in the two-stream model are more reflective and have a higher transmittance than the leaves themselves (Dorman & Sellers, 1989; Oleson *et al.*, 2004). This scheme appears to adequately simulate the behavior of Mediterranean grassland but clearly not that of more temperate sites. We surmise that at the temperate sites studied here, senescing material does not accumulate (because of grazing or decomposition) to a stem area index of ~ 2, as used in the model, or the material does not have the optical properties specified. None of the models using fixed albedos (Table 2) adopt such high summer grassland values.

Implications for LSM

Errors in albedo will translate into LSM biases in sensible and latent heat production, except where errors in grid cells composed of multiple vegetation types are offsetting. Because of the nonrandom global distribution of PFTs, errors in albedo of a specific PFT can thus lead to regional warm or cold biases of climate models incorporating these PFTs. One potential bias is the NDT PFT in models using the two-stream albedo approach. The NDT is the dominant PFT in eastern Siberia, so underestimating the albedo of this type would lead to a summer warm bias applied to a region that covers $2 \times 10^6\,\mathrm{km}^2$. The over-estimate of grassland albedos can have similar regional effects, but in the opposite direction. We note that the albedo of the arctic grass PFT in the two-stream model is simulated identically to the temperate grassland PFT, and would thus likely be too high.

Our results suggest that some re-examination may be necessary for climate model studies that have calculated the climatic impacts of afforestation or deforestation schemes where grasslands are exchanged for conifer forests (e.g. Betts, 2000; Gibbard *et al.*, 2005; Bala *et al.*, 2007). In these studies, the climatic warming caused by the lower albedo of conifer forests compared with grasslands overwhelmed the cooling effect of forest carbon sequestration. Although some of the climatic impact of such biome conversion scenarios occurs in early spring when grasslands are snow covered and consequently exhibit a very high albedo, some of the impact is likely due to growing season differences in albedo. We suggest that growing season albedos were overestimated for grasslands in some of these studies (e.g. Gibbard *et al.*, 2005; Bala *et al.*, 2007) or underestimated for deciduous conifer forests (Betts, 2000; Gibbard *et al.*, 2005; Bala *et al.*, 2007), and that a consequence of these mis-specified albedos will be an over estimate of the climatic warming resulting from a switch from grassland to forests in these models.

Improving two-stream model parameter estimates

Model inversion techniques are used to estimate parameters that allow model results to best reproduce a dataset. We used this approach to determined model parameters of the two-stream albedo model based on 2 weeks of mid-summer half-hourly data with fixed values of leaf and stem area index (Bonan, 1996). By calculating the scattering coefficient as a weighted sum of foliage and stem optical properties [see Eqn (6)], the two-stream model approach creates a perfect tradeoff (inverse correlation) between foliage and stem optical parameters. This high degree of correlation means that all nine parameters for a vegetation type cannot be simultaneously estimated. Additionally, the scattering coefficient in the two-stream model is a sum of foliage reflection and transmittance, further limiting the ability to estimate independent parameters. To make the problem tractable, we fixed stem optical properties to values in Dorman & Sellers (1989) and estimated five parameters; leaf visible and NIR reflectance and transmittance, and the leaf angle deviation from random (α_{vis}, α_{NIR}, τ_{vis}, τ_{NIR}, and χ).

We show estimates of the best-fit parameters for the BDT-TEM, NET, and NDT PFTs based on data from Howland and Bartlett forests and a larch stand near Howland (Fig. 6). The point clouds in Fig. 6 represent the best-fit parameter and 95% confidence intervals. The default parameter values used in the model for these PFTs (Dorman & Sellers, 1989) (the isolated circles and triangles in Fig. 6) do not lie within the 95% region for any parameter. (Note that the parameter values for NET and NDT are the same in the two-stream model.) An important result apparent in Fig. 6 is that the

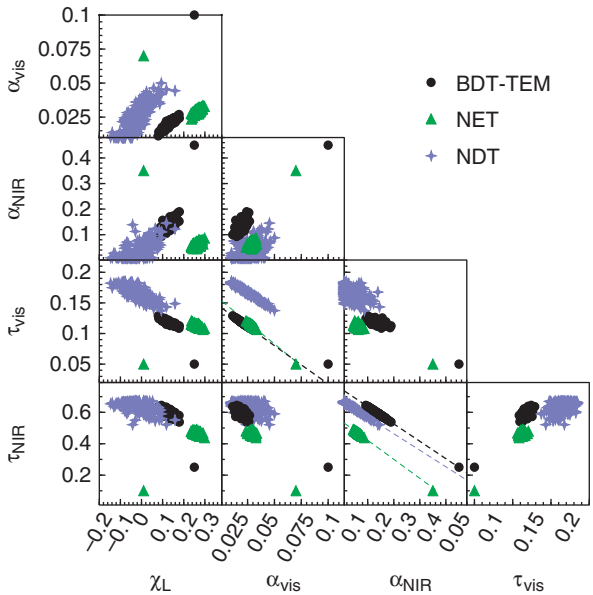

Fig. 6 Values for two-stream albedo model parameters estimated by model inversions. Black dots indicate the temperate deciduous broadleaf forest, green triangles a sub-boreal conifer forest, and blue crosses a deciduous conifer forest. The isolated dot and triangle in each panel represent the default model parameter values for the BDT-TEM and NET functional types (the default NDT parameters are identical to NET values).

parameters are not independent; all of the parameters in each case (and for each PFT) are positively or negatively correlated with all others of that PFT (i.e. BDT-TEM α_{vis}, is correlated with BDT-TEM α_{NIR}, τ_{vis}, τ_{NIR}, and χ). The correlations range from a minimum r of 0.31 (NET τ_{vis}: τ_{NIR}) to an almost exact negative correlation ($r = -0.99$) between α_{vis} and τ_{vis}, and α_{NIR} and τ_{NIR} for all three PFTs. The high degree of correlation between parameters means that many different combinations of parameter values can do an equally good job of generating the same albedos and matching the field data (within its uncertainty). Interestingly, for both the BDT-TEM and NET PFTs, the default α_{NIR} and τ_{NIR} coefficients lie on the line defined by α_{NIR}/τ_{NIR} in the inversion solutions. This means that the albedos and variation in albedo generated by the model with the default parameter pair will do an almost equally good job of matching those recorded in the field compared with the optimized parameters. A sensitivity analysis (Table 3) of the two-stream model provides further evidence that albedo is a function of the overall scattering rather than of any parameter. The change in albedo is proportionally sensitive to the change in the summed optical parameters (or the proportion of that total manifest by a change in the individual parameters), not of the individual parameters themselves.

Table 3 Sensitivity of two-stream model albedo to variation in foliage and foliage angle distribution parameters

	% Change in base albedo (0.153) for 10% change in parameter		
Parameter	Nominal value	−10% parameter	+10% parameter
α_{vis}	0.1	−0.8	0.8
α_{NIR}	0.45	−9.2	10.2
τ_{vis}	0.05	−0.3	0.3
τ_{NIR}	0.25	−4.8	5.1
χ	0.1 (0.1 → 0.01)	−1.1 (0.1 → 0.25)	2.3

Results presented for broad-leaf evergreen tree (BET) functional type in mid-summer (integrated albedo between days 196 and 210), radiation and solar angle data based on values from Bartlett Forest. Results for other PFTs and at other times of the year are similar. For χ, the leaf angle distribution, results are shown for changing the parameter associated with a BET plant functional type to that of a NET or BDT type.
BDT, broadleaf deciduous trees; NET, needle-leaf evergreen trees.

The utility of parameter estimation in the two-stream model is limited by the model approach of summing different values of leaf area index and stem area index (each with their distinct optical properties) throughout the year. Although optimum parameters can be estimated for any time when leaf and stem area index are fixed, different amounts of foliage and stems will result in different parameter estimates through the season, reducing their usefulness. Instead, we explore in a later section another approach of allowing two-stream model parameters to vary as a function of nitrogen concentrations at the top of the canopy.

Generality of the albedo-nitrogen relationship

The results based on tower albedo and foliage nitrogen measurements provide strong support for the recent findings of Ollinger *et al.* (2008) who identified a canopy nitrogen–albedo relationship in data from the Airborne Visible and InfraRed Imagine Spectrometer (AVIRIS; calibrated to field-measured %N and used to determine spatially averaged %N for tower footprints) and the Moderate Resolution Imaging Spectrometer (MODIS; used for albedo in the corresponding locations). When leaf area index is high and below a nitrogen concentration of ~2.5%, both Ollinger *et al.* (2008) and this dataset show a strong linear relationship with similar slopes; here, a foliage nitrogen change from 1% to 2% resulted in an albedo increase of 0.067, in Ollinger *et al.* (2008) who limited their analysis to forests, the same change in nitrogen increased albedo by 0.05. Based on

albedo data from several soybean fields (Fig. 4), the tower-based results suggest that the N : albedo relationship saturates at high foliage N concentrations. We caution that neither this nor our previous work contain data from tropical forests, or arctic tundra or shrubs. However, based on albedo and typical foliage N values available in the literature (e.g. Reich *et al.*, 1991; Garnier *et al.*, 1997; Michelsen *et al.*, 1996) it is likely that the %N-albedo relationship for these other PFTs will be consistent with that predicted by our Fig. 4.

Physical mechanism underlying the leaf nitrogen canopy albedo relationship

The optical properties of leaves have long been known to derive from light scattering at internal interfaces and absorption by pigments (see Woolley, 1971 for overview). Leaves absorb most of the radiation that strike them in the optical wavelengths (400–700 nm) because of the presence of chlorophyll and other pigments (Gates *et al.*, 1965). These pigments absorb poorly in the infrared where photons lack sufficient energy to drive photosynthesis, so leaves reflect and transmit most incoming NIR radiation. When light moves from a medium of one refractive index to another it is both reflected and refracted (bent) as described in the Fresnel relations. If a leaf consisted of a smooth surface and homogeneous internal refractive index, most incoming NIR radiation impinging at less than near grazing angles ($< \sim 75^{\circ}$) would pass through it and be transmitted, with little reflected back toward the source of radiation. Because leaves contain air-filled intercellular spaces (refractive index 1) interspersed with mesophyll cells (refractive index ~ 1.45), radiation is reflected and refracted many times, leading to higher reflectances (and corresponding lower transmittances) in the NIR spectral region (Gates *et al.*, 1965; Woolley, 1971).

Allen *et al.* (1970a) modeled scattering by the refractive index discontinuity between mesophyll cells and intercellular air spaces in foliage using a theory based on stacked transparent plates separated by airspaces. Leaves with a greater amount of internal interfaces conceptually contain larger stacks of plates than leaves with simpler internal anatomies. As the number of plates (scattering) increases, more radiation is reflected from the leaf and correspondingly less is transmitted. Jacquemoud & Baret (1990) incorporated this plate model into their successful PROSPECT model of leaf optical properties. When coupled to a canopy model such as SAIL (Verhoef, 1984) which tracks both forward scattering (transmittance) and back scattering (reflectance) separately, increasing the internal scattering of leaves (increasing the number of plates via the 'leaf mesophyll structure index') increases canopy reflectance for all wavelengths (Fig. 7a). The important aspect of increased scattering is in the initial interaction of photons with foliage; as the increased reflectance is at the upper boundary of the canopy, it results in a direct enhancement of canopy albedo. Lower in the canopy the radiation becomes more isotropic because of transmittance from layers above and multiple reflections, so the impact of enhanced leaf scattering on overall canopy albedo becomes small.

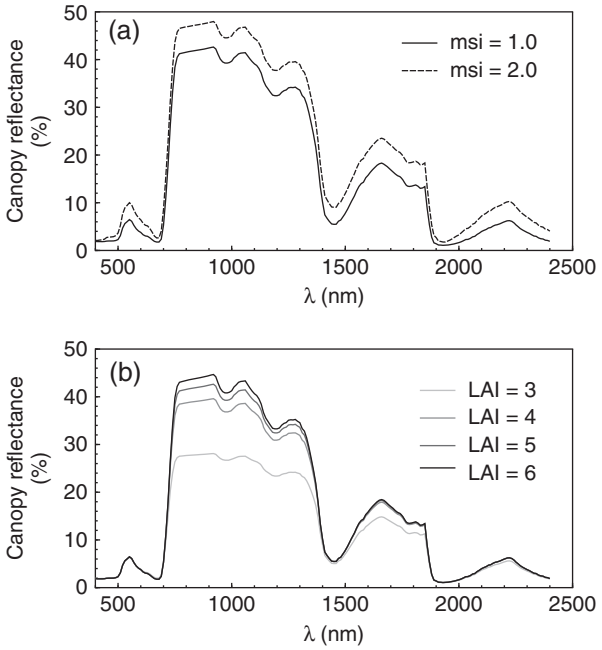

Fig. 7 Canopy reflectance values calculated via the Prospect-SAIL model (WinSail). (a) Increasing leaf scattering in the PROSPECT leaf model (changing mesophyll surface index, msi) increases canopy reflectance calculated via SAIL. (b) Increasing leaf area index (LAI) has a decreasing effect on reflectance and is only significant in the near infrared.

The question is why should leaf scattering rise with nitrogen? Previously (Ollinger *et al.*, 2008), we hypothesized that the nitrogen–albedo correlation results from how leaf structure covaries with leaf function. This involves two well-known associations between form and function; that between leaf nitrogen and photosynthetic capacity (e.g. Field & Mooney, 1986; Reich *et al.*, 1997), and that between internal leaf structure and photosynthetic capacity. The photosynthetic capacity of leaves is related to their nitrogen content because most foliage nitrogen is in the RuBP carboxylase and pigment–protein complexes that carry out photosynthesis (Evans, 1989). High rates of leaf photosynthesis require corresponding changes in internal leaf structure to permit rapid diffusion of CO_2 to the sites of photosynthesis. One of the most important of these changes (Nobel *et al.*, 1975; Longstreth *et al.*, 1985) is an increase

in the ratio of leaf mesophyll cell surface area exposed to intercellular air spaces per unit leaf area (A_{mes}/A). Slaton *et al*. (2001) investigated plant anatomy in relation to NIR reflectance and found a strong correlation between NIR leaf reflectance and A_{mes}/A, putting the relationship between scattering and internal structure described by earlier workers (e.g. Woolley, 1971) on a firm quantitative basis. Factors other than A_{mes}/A such as leaf thickness and type of mesophyll structure also vary with photosynthetic capacity (Smith *et al*., 1997) and likely also affect leaf scattering and hence albedo. It is interesting to observe how suites of characters that evolved to address leaf-scale processes interact to affect properties of the land surface boundary of the climate system. If this mechanism is correct, it seems likely that scattering could be uncoupled from foliage nitrogen concentration and become a target for breeding to produce climate friendly, higher albedo crops and trees (e.g. Ridgwell *et al*., 2009).

Making the two-stream albedo model sensitive to foliage nitrogen concentration

Unlike more sophisticated canopy radiation models (e.g. Fig. 7), the Sellers (1985) two-stream model does not separately track forward and back scattering; scattering is assumed isotropic. Thus, albedo calculated from the two-stream model is insensitive to the proposed mechanism where increasing leaf nitrogen is associated with foliage structural changes that result in increased back scattering. To implement such sensitivity, another approach is needed. The simplest approach (while not biologically or physically realistic) is to relate total leaf scattering (the sum of reflectance and transmittance) to nitrogen. The high degree of parameter correlation (Fig. 6) and examination of the two-stream model formulation shows the high redundancy in optical parameters in this model and suggests that the model can be reformulated with fewer parameters with little or no loss in predictive ability. By holding most other parameters fixed, we can invert the model and solve for how a single parameter (α_{NIR}) should vary as a function of nitrogen content to reproduce the albedos recorded at the various tower sites (Fig. 8a). Nitrogen in this way sets a maximum albedo that can be achieved; the actual albedo will also depend upon leaf area index, solar elevation, the ratio of direct to diffuse radiation, the leaf angle distribution and the amount of stem material present.

The result is surprising; when the leaf NIR parameter is set in this way, most of the albedo variation between and within PFTs observed in the data (Figs 2 and 3) can be replicated by the two-stream model when given the appropriate foliage nitrogen content and leaf area index

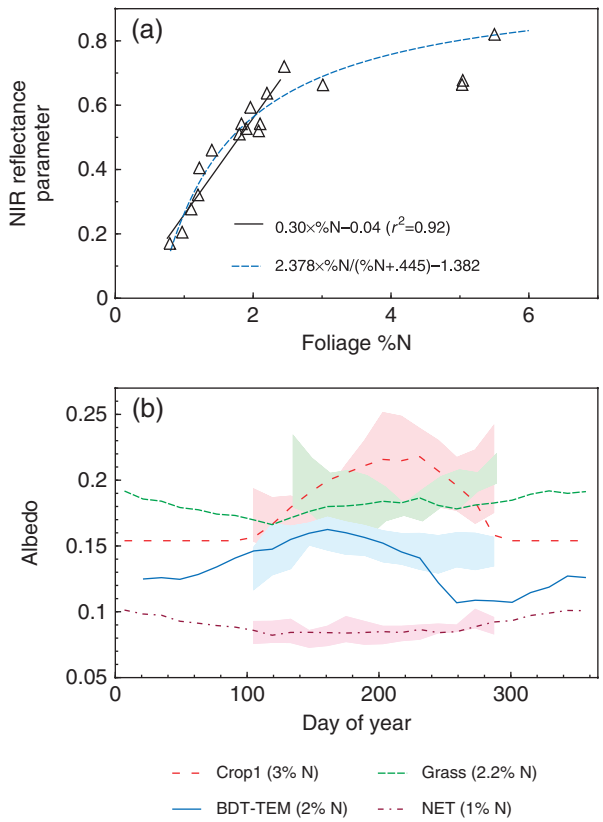

Fig. 8 (a) Near infrared parameter estimates for the two-stream model as a function of foliage nitrogen at the top of the canopy. (b) Two-stream model albedo estimates based on the nitrogen relationship shown at top and the nitrogen values shown in the legend. The shaded areas represent the 95% confidence intervals for the field measurements of crops (red), grass (green), broadleaf deciduous trees (blue), and conifers (maroon). The seasonal variation in albedo within each plant functional type (PFT) is driven primarily by variation in leaf area index as described in Bonan (1996). The variation between PFT is set by foliage %N.

(Fig. 7b). At low values of nitrogen, the relationship between %N and α_{NIR} is linear (with an intercept not significantly different from 0), saturating as would be expected at high nitrogen. Because of the additive structure of the two-stream model, the coefficients of these relationships between %N and α_{NIR} in Fig. 8a are only valid when the other leaf parameters are fixed at the following values; $\alpha_{vis} = 0.10$, $\tau_{vis} = 0.05$, $\tau_{NIR} = 0.15$ (stem optical properties are left fixed at default values for trees and changed to equal foliage properties for grasses and crops).

Conclusion

Comparison of a tower-based albedo dataset to values used in the land surface component of various climate models shows generally good agreement. However, some

models utilized values for some PFTs that are inconsistent with observations. The parameterization of grasslands and NDTs in the two-stream model appear in error.

We found strong support for the direct and pervasive relationship between surface albedo and top of canopy foliage nitrogen concentration we reported previously (Ollinger *et al.*, 2008). However, here we use both different measurements (tower-based albedo and direct foliar analysis) and extended this relationship into additional vegetation types. We also expand on the mechanism for this relationship, hypothesizing that the key is increased *back*scattering that results from coordinated internal structural changes necessary to support increased photosynthetic rates made possible by increasing nitrogen levels. The albedo–nitrogen relationship has been incorporated into simple variation of a single parameter of the widely used two-stream radiation model, and we suggest that those land surface and global climate models in which the two-stream model appears will gain considerable utility by incorporating the foliage N-albedo relationship.

Relationships between nitrogen and photosynthesis, stomatal conductance, and canopy architecture form some of the basic tenants of modern plant ecophysiology and biogeography (Leuning *et al.*, 1995; Sellers *et al.*, 1997; Bonan, 2008) and provide a foundation for the next generation of LSMs (e.g. Friend & Kiang, 2005; Thornton & Zimmermann, 2007). The present results will be useful in tying the nitrogen cycle to surface radiant energy exchange.

Acknowledgements

We thank the Northeast Wilderness Trust and GMO, LLC for providing access to the research site in Howland, Maine. This research was supported by the Office of Science (BER), US Department of Energy, Interagency Agreement No. DE-AI02-07ER64355, and NASA's Carbon Cycle Science Program and Interdisciplinary Science Program with contributions from the Harvard Forest and Hubbard Brook Long-Term Ecological Research programs and the USDA Forest Service Northern Research Station.

References

Allen WA, Gausman HW, Richardson AJ (1970a) Mean effective optical constants of cotton leaves. *Journal of the Optical Society of America*, **60**, 542–547.

Allen WA, Gayle TV, Richardson AJ (1970b) Plant-canopy irradiance specified by the Duntley equations. *Journal of the Optical Society of America*, **60**, 372–376.

Asner GP (1998) Biophysical and biochemical sources of variability in canopy reflectance. *Remote Sensing of the Environment*, **64**, 234–253.

Bala G, Caldeira K, Wickett M, Phillips TJ, Lobell DB, Delire C, Mirin A (2007) Combined climate and carbon-cycle effects of large-scale deforestation. *Proceedings of the National Academy of Science*, **104**, 6550–6555.

Baldocchi D, Falge E, Gu L *et al.* (2001) FLUXNET: a new tool to study the temporal and spatial variability of ecosystem-scale carbon dioxide, water vapor and energy flux densities. *Bulletin of the American Meteorological Society*, **82**, 2415–2434.

Baldocchi DD, Xu L, Kiang N (2004) How plant functional-type, weather, seasonal drought, and soil physical properties alter water and energy fluxes of an oak–grass savanna and an annual grassland. *Agricultural and Forest Meteorology*, **123**, 13–39.

Betts AK, Ball JH (1997) Albedo over the boreal forest. *Journal of Geophysical Research*, **102** (D24), 28901–28909.

Betts RA (2000) Offset of the potential carbon sink from boreal forestation by decreases in surface albedo. *Nature*, **408**, 187–190.

Bonan GB (1996) *A land surface model (LSM version 1.0) for ecological, hydrological, and atmospheric studies: Technical description and user's guide*. NCAR Technical Note, NCAR/TN-417 + STR, January 1996, 150 pp.

Bonan GB (1997) Effects of land use on the climate of the United States. *Climatic Change*, **37**, 449–486.

Bonan GB (2008) Forests and climate change: forcings, feedbacks, and the climate benefits of forests. *Science*, **320**, 1444–1449.

Bonan GB, Oleson KW, Vertenstein M *et al.* (2002) The land surface climatology of the community land model coupled to the NCAR community climate model. *Journal of Climate*, **15**, 3123–3149.

Bonan GB, Pollard D, Thompson SL (1992) Effects of boreal forest vegetation on global climate. *Nature*, **359**, 716–718.

Coakley JA Jr, Chýlek P (1975) The two-stream approximation in radiative transfer: including the angle of the incident radiation. *Journal of the Atmospheric Sciences*, **32**, 409–418.

Cook BD, Davis KJ, Wang W *et al.* (2004) Carbon exchange and venting anomalies in an upland deciduous forest in northern Wisconsin, USA. *Agricultural and Forest Meteorology*, **126**, 271–295, doi: 10.1016/j.agformet.2004.06.008.

Cox PM, Betts RA, Bunton CB, Essery RLH, Rowntree PR, Smith J (1999) The impact of new land surface physics on the GCM simulation of climate and climate sensitivity. *Climate Dynamics*, **15**, 183–203.

Dai Y, Zeng Q-C (1997) A land surface model (IAP94) for climate studies. Part I: formulation and validation in off-line experiments. *Advances in Atmospheric Sciences*, **14**, 433–460.

Dai Y, Zeng X, Dickinson RE *et al.* (2003) The common land model. *Bulletin of the American Meteorological Society*, **84**, 1013–1023.

Dickinson RE (1983) Land surface processes and climate-surface albedos and energy balance. *Advances in Geophysics*, **25**, 305–353.

Dickinson RE, Henderson-Sellers A, Kennedy PJ, Wilson MF (1986) *Biosphere–Atmosphere Transfer Scheme (BATS) for the NCAR Community Climate Model*. NCAR Technical Note. NCAR/TN-275 + STR. National Center for Atmospheric Research, Boulder, CO, 69 pp.

Dorman JL, Sellers PJ (1989) A global climatology of albedo, roughness length and stomatal resistance for atmospheric general circulation models as represented by the Simple Biosphere model (SiB). *Journal of Applied Meteorology*, **28**, 833–855.

Evans JR (1989) Photosynthesis and nitrogen relationships in leaves of C3 plants. *Oecologia*, **78**, 9–19.

Federer CA (1968) Spatial variation of net radiation, albedo and surface temperature of forests. *Journal of Applied Meteorology*, **7**, 789–795.

Field C, Mooney HA (1986) The photosynthesis–nitrogen relationship in wild plants. In: *On the Economy of Plant Form and Function* (ed. Givnish TJ), Cambridge University Press, Cambridge, UK.

Foley JA, Prentice IC, Ramankutty N *et al.* (1996) An integrated biosphere model of land surface processes, terrestrial carbon balance, and vegetation dynamics. *Global Biogeochemical Cycles*, **10**, 603–628.

Friend AD, Kiang NY (2005) Land surface model development for the GISS GCM: effects of improved canopy physiology on simulated climate. *Journal of Climate*, **18**, 2883–2902.

Garnier E, Cordonnier P, Guillerm J-L, Sonié L (1997) Specific leaf area and leaf nitrogen concentration in annual and perennial grass species growing in Mediterranean old-fields. *Oecologia*, **111**, 490–498.

Gates DM, Keegan HJ, Schleter JC, Weidner VR (1965) Spectral properties of plants. *Applied Optics*, **4**, 11–20.

Gibbard S, Caldeira K, Bala G, Phillips TJ, Wickett M (2005) Climate effects of global land cover change. *Geophysical Research Letters*, **32**, L23705, doi: 10.1029.

Gough CM, Vogel CS, Schmid HP, Su H-B, Curtis PS (2008) Multi-year convergence of biometric and meteorological estimates of forest carbon storage. *Agricultural and Forest Meteorology*, **148**, 158–170.

Goulden ML, Winston GC, McMillan AMS *et al*. (2006) An eddy covariance mesonet to measure the effect of forest age on land-atmosphere exchange. *Global Change Biology*, **12**, 2146–2162.

Gu L, Meyers T, Pallardy SG *et al*. (2006) Direct and indirect effects of atmospheric conditions and soil moisture on surface energy partitioning revealed by a prolonged drought at a temperate forest site. *Journal of Geophysical Research*, **111**, D16102, doi: 10.1029/2006JD007161.

Gueymard C (2004) The sun's total and spectral irradiance for solar energy applications and solar radiation models. *Solar Energy*, **76**, 423–453.

Henderson-Sellers A, Dickinson RE, Kennedy PJ, McGuffie K, Pitman AJ (1993) Tropical deforestation: modeling local to regional-scale climate change. *Journal of Geophysical Research*, **98**, 7289–7315.

Henderson-Sellers A, Wilson MF, Thomas G, Dickinson RE (1986) *Current Global Land-Surface Data Sets for Use in Climate-Related Studies*. NCAR Technical Note. NCAR/TN-272 + STR, National Center for Atmospheric Research, Boulder, CO, 110 pp.

Hollinger DY, Aber J, Dail B *et al*. (2004) Spatial and temporal variability in forest–atmosphere CO_2 exchange. *Global Change Biology*, **10**, 1689–1706.

Jacquemoud S, Baret F (1990) PROSPECT: a model of leaf optical properties spectra. *Remote Sensing of Environment*, **34**, 75–91.

Jenkins JP, Richardson AD, Braswell BH, Ollinger SV, Hollinger DY, Smith M-L (2007) Refining light-use efficiency calculations for a deciduous forest canopy using simultaneous tower-based carbon flux and radiometric measurements. *Agricultural and Forest Meteorology*, **143**, 64–79.

Kubelka J (1948) New contributions to the optics of intensely light-scattering materials. Part I. *Journal of the Optical Society of America*, **38**, 448–457.

Kucharik CJ, Foley JA, Delire C *et al*. (2000) Testing the performance of a dynamic global ecosystem model: water balance, carbon balance, and vegetation structure. *Global Biogeochemical Cycles*, **14**, 795–825.

Law BE, Falge E, Gu L *et al*. (2002) Environmental controls over carbon dioxide and water vapor exchange of terrestrial vegetation. *Agricultural and Forest Meteorology*, **113**, 97–120.

Leuning R, Kelliher FM, De Pury DGG, Schulze E-D (1995) Leaf nitrogen, photosynthesis, conductance and transpiration: scaling from leaves to canopies. *Plant, Cell and Environment*, **18**, 1183–1200.

Longstreth DJ, Bolaños JA, Goddard RH (1985) Photosynthetic rate and mesophyll surface area in expanding leaves of *Alternanthera philoxeroides* grown at two light levels. *American Journal of Botany*, **72**, 14–19.

Manabe S (1969) Climate and the ocean circulation: I. The atmospheric circulation and the hydrology of the earth's surface. *Monthly Weather Review*, **97**, 739–774.

Mathews E (1984) *Prescription of land-surface boundary conditions in GISS GCM II: A simple method based on fine resolution data bases*. NASA Tech. Memo. 86096, June 1984, 21 pp.

Michelsen A, Jonasson S, Sleep D, Havström M, Callaghan TV (1996) Shoot biomass, d13C, nitrogen and chlorophyll responses of two arctic dwarf shrubs to in situ shading, nutrient application and warming simulated climate change. *Oecologia*, **105**, 1–12.

Milly PCD, Shmakin AB (2002) Global modeling of land water and energy balances. Part I: The Land Dynamics (LaD) Model. *Journal of Hydrometeorology*, **3**, 283–299.

Myneni RB, Ross J, Asrar G (1989) A review on the theory of photon transport in leaf canopies. *Agricultural and Forest Meteorology*, **45**, 1–153.

Nobel PS, Zaragoza LJ, Smith WK (1975) Relation between mesophyll surface area, photosynthetic rate, and illumination level during development for leaves of *Plectranthus parviflorus* Henckel. *Plant Physiology*, **55**, 1067–1070.

Oki T, Sud YC (1998) Design of total runoff integrating pathways (TRIP) – A global river channel network. *Earth Interactions*, **2**, 1–37.

Oleson KW, Dai Y, Bonan G *et al*. (2004) *Technical description of the Community Land Model (CLM)*. NCAR Technical Note, NCAR/TN-461 + STR, May 2004, 186 pp.

Ollinger SV, Richardson AD, Martin ME *et al*. (2008) Canopy nitrogen, carbon assimilation and albedo in temperate and boreal forests: functional relations and potential climate feedbacks. *PNAS*, **105**, 19335–19340.

Paw UKT, Falk M, Suchanek TH *et al*. (2004) Carbon dioxide exchange between an old growth forest and the atmosphere. *Ecosystems*, **7**, 513–524.

Pitman AJ (2003) The evolution of, and revolution in, land surface schemes designed for climate models. *International Journal of Climatology*, **23**, 479–510.

Randall DA, Wood RA, Bony S *et al*. (2007) Climate models and their evaluation. In: *Climate Change 2007: The Physical Science Basis. Contribution of Working Group I to the Fourth Assessment Report of the Intergovernmental Panel on Climate Change* (eds Solomon S, Qin D, Manning M, Chen Z, Marquis M, Averyt KB, Tignor M, Miller HL), pp. 591–662. Cambridge University Press, Cambridge, UK.

Reich PB, Uhl C, Walters MB, Ellsworth DS (1991) Leaf lifespan as a determinant of leaf structure and function among 23 amazonian tree species. *Oecologia*, **86**, 16–24.

Reich PB, Walters MB, Ellsworth DS (1997) From tropics to tundra: global convergence in plant functioning. *Proceedings of the National Academy of Science*, **94** (25), 13730–13734.

Ridgwell A, Singarayer JS, Hetherington AM, Valdes PJ (2009) Tackling regional climate change by leaf albedo bio-geoengineering. *Current Biology*, **19**, 146–150.

Ross J (1981) *The Radiation Regime and Architecture of Plant Stands*. Dr Junk, The Hague.

Schaeffer M, Eickhout B, Hoogwijk M *et al*. (2006) CO_2 and albedo climate impacts of extratropical carbon and biomass plantations. *Global Biogeochemical Cycles*, **20**, 1–15.

Schmid HP, Grimmond CSB, Cropley F, Offerle B, Su HB (2000) Measurements of CO_2 and energy fluxes over a mixed hardwood forest in the mid-western United States. *Agricultural and Forest Meteorology*, **103**, 357–374.

Sellers P (1985) Canopy reflectance, photosynthesis and transpiration. *International Journal of Remote Sensing*, **6**, 1335–1372.

Sellers PJ, Dickinson RE, Randall DA *et al*. (1997) Modeling the exchanges of energy, water, and carbon between continents and the atmosphere. *Science*, **275**, 502–509.

Sellers PJ, Dorman JL (1986) Testing the simple biosphere model (SiB) using point micrometeorological and biophysical data. *Journal of Climate and Applied Meteorology*, **26**, 622–651.

Sellers PJ, Randall DA, Collatz GJ *et al*. (1996) A revised land surface parameterization (SiB_2) for atmospheric GCMs. Part 1: model formulation. *Journal of Climate*, **9**, 676–705.

Skowronski N, Clark K, Nelson R, Hom J, Patterson M (2007) Remotely sensed measurements of forest structure and fuel loads in the Pinelands of New Jersey. *Remote Sensing of Environment*, **108**, 123–129.

Slaton MR, Hunt ER Jr, Smith WK (2001) Estimating near-infrared leaf reflectance from leaf structural characteristics. *American Journal of Botany*, **88**, 278–284.

Smith WK, Vogelmann TC, DeLucia EH, Bell DT, Shepherd KA (1997) Leaf form and photosynthesis. *BioScience*, **47**, 785–793.

Stoy PC, Katul GG, Siqueira MBS *et al*. (2005) Variability in net ecosystem exchange from hourly to inter-annual time scales at adjacent pine and hardwood forests: a wavelet analysis. *Tree Physiology*, **25**, 887–902.

Suits GH (1972) The calculation of the directional reflectance of a vegetative canopy. *Remote Sensing of Environment*, **2**, 117–125.

Tarantola A (2005) *Inverse Problem Theory and Methods for Model Parameter Estimation*. Society for Industrial and Applied Mathematics, Philadelphia, PA, USA.

Thornton PE, Zimmermann NE (2007) An improved canopy integration scheme for a land surface model with prognostic canopy structure. *Journal of Climate*, **20**, 3902–3923.

Verhoef W (1984) Light scattering by leaf layers with application to canopy reflectance modeling: The SAIL model. *Remote Sensing of Environment*, **16**, 125–141.

Verma SB, Dobermann A, Cassman KG *et al*. (2005) Annual carbon dioxide exchange in irrigated and rainfed maize-based agroecosystems. *Agricultural and Forest Meteorology*, **131**, 77–96.

Woolley JT (1971) Reflectance and transmittance of light by leaves. *Plant Physiology*, **47**, 656–662.